Riverine flood risk assessment with a combined model chain in southeastern China

Shenghui Cui[1], Lihong Wang[1], Jianxiong Tang[2], Lei Fang[3], Xuejuan Fang[1], Sabita Shrestha[1], Bikram Manandhar[1], Jinliang Huang[4], and Vilas Nitivattananon[5]

[1]Institute of Urban Environment Chinese Academy of Sciences
[2]Xiamen Municipal Government
[3]Xi'an University of Architecture and Technology
[4]Xiamen University
[5]Asian Institute of Technology School of Engineering and Technology

February 10, 2023

Abstract

Climate change and rapid urbanization have exacerbated the occurrence and impact of floods. It is essential to carry out a quantitative flood risk assessment and manage the flood risk before a disaster occurs. This article presents a combined riverine flood risk model to obtain the exceedance probability loss (EPL) curve and expected annual damage (EAD) under the current climate. This model includes a rapid flood model and a flood damage model. It aims to simulate the flood risk and evaluate the flood damage at 10-, 30-, 50-, 100-, and 200-year return period events. The results show that: (1) The total inundation areas will sharply increase when the flood return periods are over 30 years. (2) The EAD is 1,476 million dollars in the Jiulong River Basin (JRB). When the flood return period is over 30 years, the total damage increases sharply. (3) The flood risk in the lower reaches of the JRB is higher than in the upper reaches when the flood event is beyond a 20-year return period. (4) Industrial sector damage is the largest, followed by tertiary industry, transportation, construction, agriculture, and infrastructure. This study will provide actionable information for future flood risk management, and this combined model chain is also suitable for other similar river basins.

Riverine flood risk assessment with a combined model chain in southeastern China

Lihong Wang[1,2,3] , Shenghui Cui[1,3], Jianxiong Tang[4], Lei Fang[5], Xuejuan Fang[1,2,3], Sabita Shrestha[1,2,3], Bikram Manandhar[1,2,3,8] Jinliang Huang[6], Vilas Nitivattananon[7]

Shenghui Cui

shcui@iue.ac.cn

1 Key Laboratory of Urban Environment and Health, Institute of Urban Environment, Chinese Academy of Sciences, Xiamen 361021, China

2 University of Chinese Academy of Sciences, Beijing 100049, Xiamen Key Lab of Urban Metabolism, Xiamen 361021, China

3 Xiamen Key Lab of Urban Metabolism, Institute of Urban Environment, Chinese Academy of Sciences, Xiamen 361021, China

4 Xiamen Municipal Natural Resources and Planning Bureau, Xiamen 361012, China

5 Xi'an University of Architecture and Technology, School of Public Administration, Xi'an 710000, China

6 Fujian Key Laboratory of Coastal Pollution Prevention and Control, Xiamen University, Xiamen 361102, China

7 Department of Development and Sustainability, School of Environment, Resources and Development, Asian Institute of Technology, Pathumthani 12120, Thailand

8 Tribhuvan University, Institute of Forestry, Hetauda 44107, Nepal

Abstract: Climate change and rapid urbanization have exacerbated the occurrence and impact of floods. It is essential to carry out a quantitative flood risk assessment and manage the flood risk before a disaster occurs. This article presents a combined riverine flood risk model to obtain the exceedance probability loss (EPL) curve and expected annual damage (EAD) under the current climate. This model includes a rapid flood model and a flood damage model. It aims to simulate the flood risk and evaluate the flood damage at 10-, 30-, 50-, 100-, and 200-year return period events. The results show that: (1) The total inundation areas will sharply increase when the flood return periods are over 30 years. (2) The EAD is 1,476 million dollars in the Jiulong River Basin (JRB). When the flood return period is over 30 years, the total damage increases sharply. (3) The flood risk in the lower reaches of the JRB is higher than in the upper reaches when the flood event is beyond a 20-year return period. (4) Industrial sector damage is the largest, followed by tertiary industry, transportation, construction, agriculture, and infrastructure. This study will provide actionable information for future flood risk management, and this combined model chain is also suitable for other similar river basins.

Keywords: Flood return period; risk assessment; depth-damage curve; damage estimation; uncertainty

1. Introduction

Flooding has become a severe natural disaster worldwide because of its frequent occurrence, widespread influence, and consequent heavy losses to human life and property (Zhang et al., 2018; Yang et al., 2020; Zhang et al., 2021a, b). According to the Emergency Events Database (EM-DAT), floods accounted for 44.28% of the 7,348 disaster events in the world from 2000 to 2019 and caused a global economic loss of up to 2.97 trillion US dollars (CRER, 2020). Riverine flooding caused by extreme rainfall will pose a huge challenge to existing infrastructure (Yildirim et al., 2021). Bloschl et al. (2017) found that riverine flooding costs an average of over $104 billion per year. Global warming is expected to cause more intense precipitation in many regions and increase the frequency and scale of flood events.(Hosseinzadehtalaei et al., 2021). With a temperature increase of 1.5 over pre-industrial levels it has been found that, depending on the socio-economic scenario, human losses from riverine flooding could rise by 70–83%, and direct flood damage could rise by 160%–240% (Dottori et al., 2018). Therefore, effectively assessing and managing flood risk is extremely important for future scientifically based disaster prevention and mitigation.

Flood risk assessment could produce flood risk management measures to reduce the impact of flood disasters on human society and the economy (Buchecker et al., 2013; Aerts et al., 2018; Wang et al., 2021b). At present, the research on flood risk assessment is divided into four categories: index system-based assessment methods, historical flood hazard-based assessment methods, flood risk assessment integrated with remote sensing (RS) and geographic information systems (GIS), and simulation-based assessment methods. Each method has its own advantages and disadvantages. The most common method for assessing flood risk is based on an index system. For example, Lyu et al. (2018) and Wang et al. (2021a) proposed a multiple index system that covers hazard, exposure, and vulnerability, to evaluate the flood risk level for future disaster management. Subsequently, Tang et al. (2021) coupled GIS and index systems and proposed a spatial multi-criteria analysis method that covers hazard, exposure, sensitivity, and adaptive capacity, to evaluate the spatiotemporal dynamics of flood risk in the Jiulong River watershed and provide visual flood risk maps for policymakers. These studies reflect flood risk dynamic changes and analyze the risk components of hazard, exposure, and vulnerability. However, an index system is highly dependent on human data-management capabilities, and the flood risk result is a relative concept. In recent years, simulation-based assessment

methods have been applied to flood risk assessment (Fernandez et al., 2010; Tehrany et al., 2014; Li et al., 2016). For example, Roy et al. (2021) used hydrology and a hydrodynamic model to estimate flood risk in the Arial Khan River. This approach can produce a simulated inundation depth map, which is gradually replacing the flood hazard map generated by the GIS platform. Thus hydrology and the hydrodynamic model are applied to simulate the flood extent and inundation depth caused by a flood event. However, this combination is limited by a complex model structure, the need for complete parameters and hydrological data, and a long calculation time (de Paiva et al., 2013; Bellos et al., 2016; Fang et al., 2022).

If an inundation map and damage can be simulated before a flood disaster occurs, the effects can be predicted and a disaster response planned. Therefore, this study presents a combined modeling approach, to express riverine flood risk at the watershed scale, while also simulating the flood progression and evaluating the flood damage. This method applies return-period scenarios at 10-, 30-, 50-, 100-, and 200-year levels, to simulate a flood map before a real flood disaster event. Additionally, this method uses the Height Above the Nearest Drainage (HAND) model to replace the hydrodynamic model, and it has overcome the problem of long calculation time. Another advantage is the ability to estimate the flood risk directly from the damage, for different return periods.

The objectives of this study were to create a flood risk curve and provide the expected annual damage (EAD) of riverine floods induced under the current climate, land use surface, and socio-economic level, in the JRB. Furthermore, the research results will produce actionable information on flood risk management to cope with increased flood risk. Section 2 presents the flood risk method. Section 3 analyzes the hazard, vulnerability, exposure, flood risk, and sector damage at 10-, 30-, 50-, 100-, and 200-year return periods in the JRB. Section 4 discusses the applicability and limitations of flood risk models and then discusses the future research directions of flood management. The conclusion of this paper is given in Section 5.

2. Data and methods

2.1. Study area

The Jiulong River Basin (Fig. 1) is located in Fujian Province (116°47' ~ 118°02', 24°13' ~ 25°51') in southeast China. The population of the JRB accounts for about 17% of the total population, 26.7% of the total economic output, and 12% of the land area in Fujian Province, playing an essential economic role in the province. The JRB has a total length of 1,923 km, a drainage area of 14,700 km^2, and an average annual runoff of 11.9 billion cubic meters. It comprises the North Stream, the South Stream, and the West Stream and eventually empties into the Taiwan Strait.

There are many hilly and mountainous areas within the basin, with hilly areas accounting for 88.75% of the basin's total area and plain areas accounting for 11.25%. It is famous more for its mountains area than its plain area, making the limited land resources in the basin very precious. The JRB belongs to the subtropical monsoon climate, meaning that it is prone to continuous rainy weather in spring. Typhoons and heavy rain often occur in summer, mainly from July to September. Flood disasters have occurred frequently in the JRB, throughout history, and the region is susceptible to typhoons, storm surges, and other disasters.

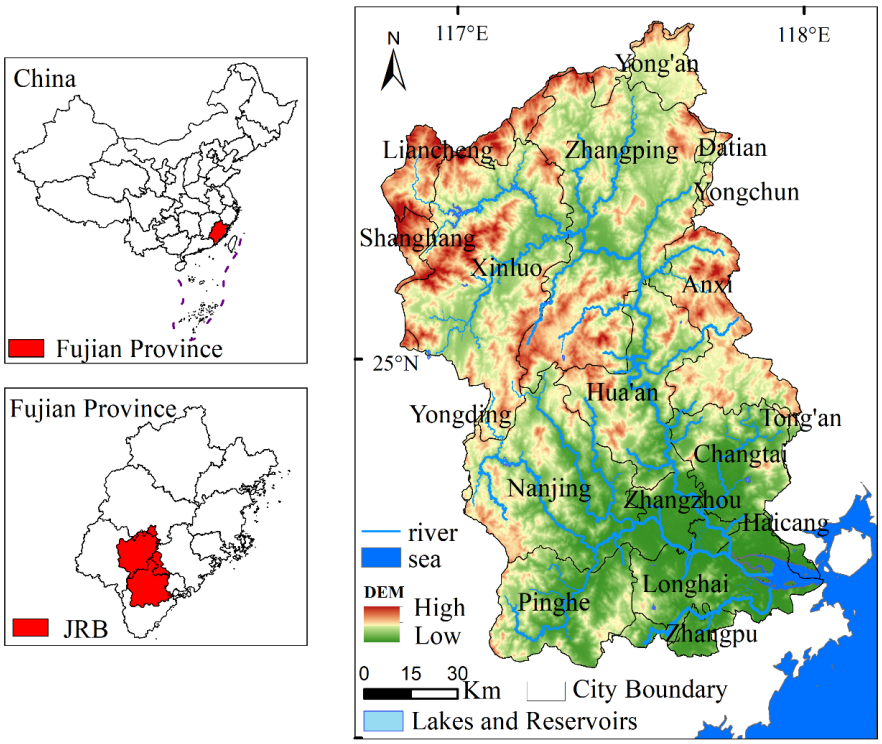

Fig. 1 Study area of Jiulong River Basin

2.2. Data sources

The socioeconomic data at the county level in 2015 were obtained from the China Statistical Yearbooks Database (CSYD; data.cnki.net). Land-use data were 30-M remote sensing images obtained from the Geographical Information Monitoring Cloud Platform (http://www.dsac.cn/DataProduct/Index/20). Land-use data were then reclassified into farmland, forestland, grassland, water body, and built-up land. The classification accuracy of cultivated land data is 85%; other data classification accuracy can reach more than 75% (Tang et al., 2020). The depth-damage curve of the cultivated land refers to the Asian damage function for agriculture (Huizinga et al., 2017), and the depth-damage curve of the built-up area was taken from the Rhine Atlas (ICPR, 2001).

2.3. Methods

2.3.1. The P-III curve and the HAND model

The current climate description was based on a 50-year record of the discharge and water-level measurements in the JRB. The P-III curve was used to fit the design discharges with five return periods (10-, 30-, 50-, 100-, and 200-year), and then, based on the record water levels, the design discharges were used to fit the stage-discharge relationship curve in the JRB. The flood peak discharge and stage-discharge relationship curves under different flood return periods were input into the HAND model to simulate the flooding inundation extents and depths for 10, 30, 50, 100, and 200 years in the JRB (Fang, 2021; Fang et al., 2022). The HAND model simulates river inundation by determining river flow and surface runoff paths (Nobre et al., 2016; Garousi-Nejad et al., 2019). The HAND model is a rapid flood model, and it is suitable for large-scale river flood simulation. Therefore, this study used the HAND model to simulate the inundation maps of riverine floods in the JRB.

2.3.2. Depth-damage curves

When calculating loss ratio and direct monetary damage, there are two methods that can be estimated through questionnaires and by referring to depth loss curves in other regions (Win et al., 2018). The questionnaire has some credibility, but most regions lack historical disaster record data. Depth-damage curves are used to describe the relation between maximum water levels and flood damage. These curves were generated for specific regions based on historical flood damage data, empirical methods, or by interviews or questionnaire collection. Depth-damage curves are more widely used than questionnaire surveys to estimate flood damage, and this is a commonly used method for estimating direct economic damage (Wu et al., 2016). However, it was difficult to fit the depth-damage curves in the JRB using only historical data. Fortunately, transferring depth-damage curves among regions is an effective method because the established the curves usually collect a large and diverse amount of survey data (Wu et al., 2021). Thus, we cited the depth-damage curve from a developed globally consistent database (Huizinga et al., 2017), which described the vulnerability of agriculture in Asia. The depth-damage curve of built-up land was developed using the Rhine Atlas database (ICPR, 2001; Merz et al., 2010).

2.3.3. Estimating the value of exposed assets

Previous studies have used gross domestic product (GDP), fixed capital, exposed population, and direct survey methods to estimate the exposure asset value (Jongman et al., 2012; Wu et al., 2014; Wu et al., 2017; Ye et al., 2019). However, social and economic conditions vary among different regions, and asset values therefore differ. This study used county-level data to calculate asset values. In addition, due to the inconsistency between watershed boundaries and administrative boundaries, the area weight was used to calculate the relevant indicators. This step aims to obtain the value of the assets per unit of various land uses in the JRB. Thus, we extracted the agricultural and built-up land areas from the land-use map and then calculated the exposed assets of agricultural and built-up land. The formulas for calculating the exposed assets are as expressed in Eq. (1) and Eq. (2):

$$E_{\mathrm{ab}} = \left(C_f + \mathrm{GDP}_{\mathrm{na}}\right)/F_b \quad (1)$$

$$E_{\mathrm{aa}} = \mathrm{GDP}_a/F_a \quad (2)$$

where E_{ab} represents the exposed assets of built-up land;E_{aa} represents the exposed assets of agricultural land;C_f represents the cumulative investments in fixed assets of non-agricultural sectors; $\mathrm{GDP}_{\mathrm{na}}$ represents the GDP in non-agricultural sectors; GDP_a represents the GDP in the agricultural sector; F_b represents the total area of built-up land; and F_a represents the total area of agricultural land. In addition, we adjusted the GDP and investments in fixed assets to the price levels of 2015. The investments in fixed assets used data integrated from 1965 to 2015, with a 5% per year discount rate.

2.3.4. A combined flood risk model chain

The flood risk model includes a rapid flood model and a flood damage model. A rapid flood model aims to acquire a flood inundation map, and it is coupled with a hydrology model and a HAND model. The damage model interactively combines three separate modules: a spatial distribution module to estimate the exposure assets, a vulnerability module of the inundation depth-damage curves, and exceedance probability for the different flood-return periods. The flood risk models integrate the inundation depth, exposed assets, depth-damage curve, and the probability of flood events. The following four steps were used for the flood risk model in this study:

a) Input the discharge and water-level relationship curves, and the peak discharges of the five return-period flood events (10-, 30-, 50-, 100-, and 200-year) to the HAND model, acquire the inundation depth in the JRB and input the flood map to the GIS platform.

b) Select suitable depth-damage curves for the different land-use classes. Then, build the relationship between inundation depth and land-use classes on the GIS platform.

c) Collect relevant socioeconomic data, such as the GDP in the agricultural and non-agricultural sectors and the investments in fixed assets from 1965 to 2015. Then, calculate the asset values of the different land-use

classes in each unit on the GIS platform.

d) Calculate total damage for each selected inundation depth according to the depth-damage curves and asset value exposed in each land use unit. Then, calculate the total damages for the 10-, 30-, 50-, 100-, and 200-year inundation maps separately. Finally, integrate the flood damage of the different return periods and the probability of flood events.

After all these steps, we can acquire the damage under each different flood-return period, and then acquire the EPL curve (risk curve). We can calculate the EAD using the area (integral) under the risk curve. In the risk model, the higher the EAD, the higher the risk. The data processing was mainly completed on a GIS platform, and the technical framework is shown in Fig. 2.

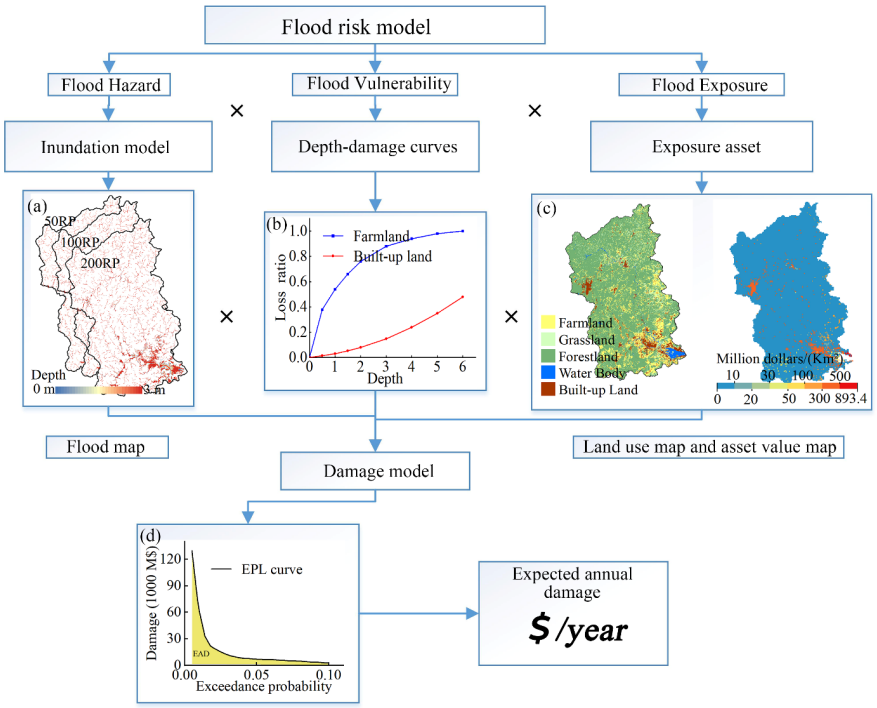

Fig. 2 Framework for flood risk assessment

3. Results

3.1. Hazard analysis

Fig. 3 shows that when the flood return period is longer than 30 years, the overall inundation areas in the basin increase sharply. The inundation areas of different land use types increase with the level of the flood return period, and the inundation area of agricultural land is the largest, followed by forests, construction land, grassland, gardens and rural residential areas. The land use map is shown in Fig. A1. The inundation areas of different land uses are shown in Fig. A2. For example, the inundation areas of agricultural land, forests, garden land, grassland, urban land, and rural residential land were 554.08 km^2, 252.17 km^2, 90.79 km^2, 109.59 km^2, 184.26 km^2, and 69.81 km^2 respectively in a 100-year return period flood. In addition, the flooded area from a 30-year return-period flood compared to that of a 50-year one showed an increase of nearly 1.7 times—the largest increase in the JRB.

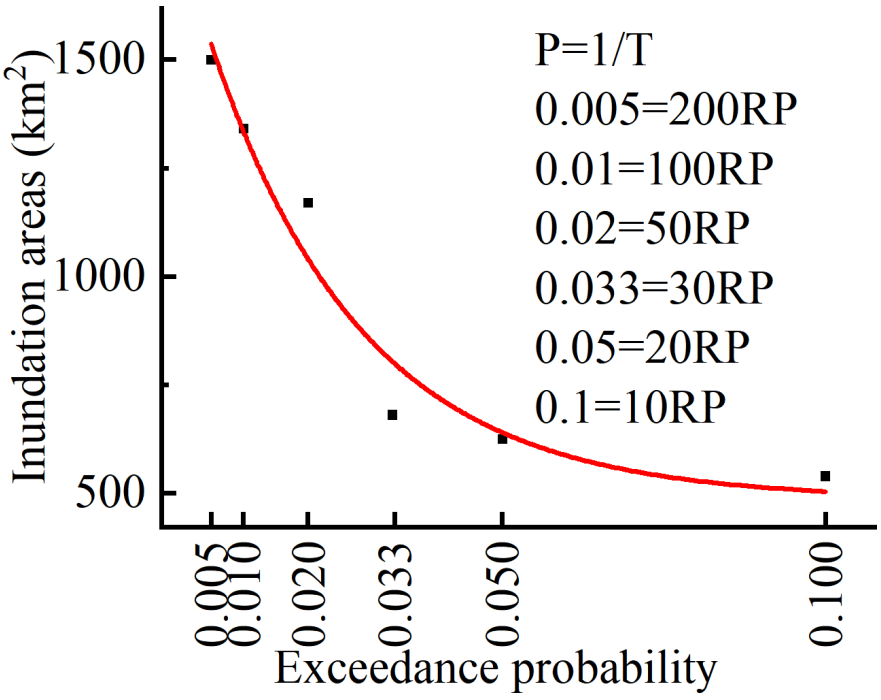

Fig. 3 Flood inundation map for different flood return periods

Note: T represents the return period of the flood event (RP). P represents the occurrence probabilities of the flood events. The flood map and the inundation areas of different land uses under different return-period floods are shown in Fig. A1, Fig. A2, and Table A1.

3.2. Vulnerability analysis

Vulnerability analyses aim to detect the relationship between loss ratio and water depth for built-up land and farmland (Yin et al., 2011). The relationships between loss ratio and water depth of built-up land and farmland are shown in Fig. 4. Fig. 4 shows that the loss ratio of farmland is usually higher than that of built-up land at the same range of inundation, indicating that farmland is more vulnerable to flood damage than built-up land. For example, when the water depth is 1 meter, the loss ratio of construction land is 0.03, while the farmland loss ratio is 0.54.

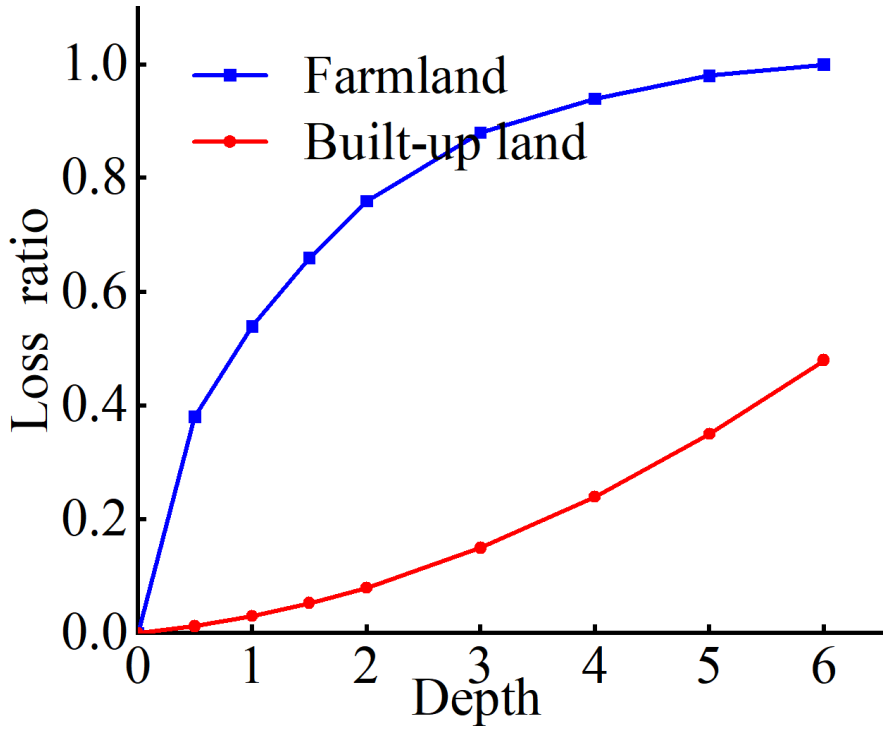

Fig. 4 Depth-damage curves for built-up land and farmland

3.3. Exposure analysis

In Fig. 5, the total exposed assets, fixed assets, and GDP in the JRB are displayed at the county scale. The largest asset exposure is in the Xinluo district, followed by Longhai city and downtown Zhangzhou. The Xinluo district is located upstream of the Jiulong River, and downtown Zhangzhou and Longhai are located downstream of the river. The unit value of built-up land is usually higher than that of farmland in the JRB (Table A2). For example, the asset value of agricultural land is 7914.24 USD (exchange rates, 1 CNY=0.157 USD) per km^2 in downtown Zhangzhou, while the asset value of construction land is 386 million USD per km^2. Although farmland is more vulnerable than built-up land, the unit value of built-up land is higher, which means that built-up land may suffer greater damage at the same inundation depth. The unit values of land in the JRB are shown in Fig. A3.

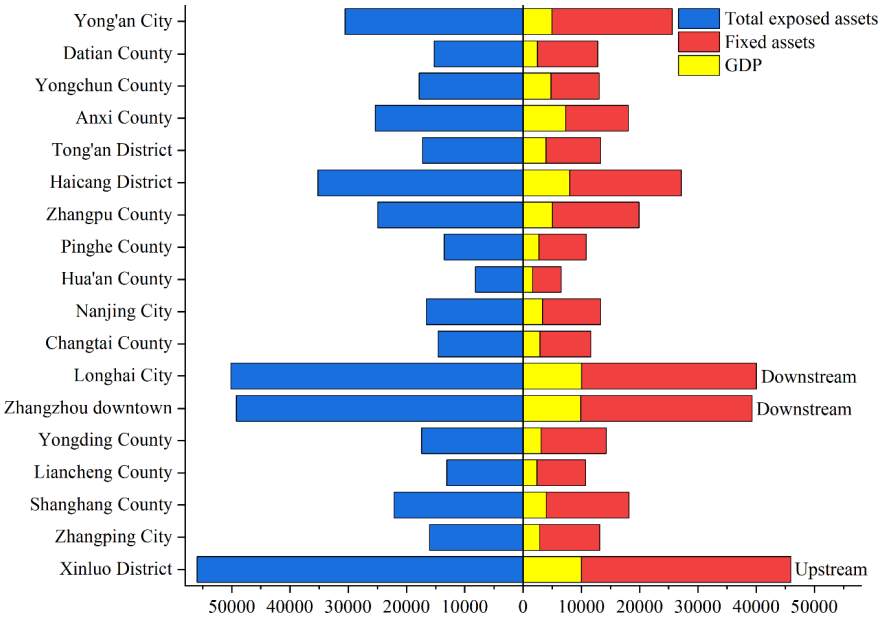

Fig. 5 Exposed assets in the JRB at the county scale (million USD)

3.4. Flood risk assessment

The damage-probability curve is named the exceedance probability loss (EPL) curve or risk curve. The EPL curve was chosen to calculate the EAD, and the EAD can be used to represent the flood risk. This study fitted the damage-probability curve based on the total damage under different return-period floods. The EAD is calculated using the area (integral) under the damage-probability curve. Fig. 6 displays the EPL curves and the EAD. From the EAD analysis, we found the riverine flood risk in the JRB to be higher, with an EAD of 147.6 million dollars every year. By analyzing China's recorded GDP and annual direct economic damage from floods from 2003 to 2019, the results show that the average annual direct economic damage of China's floods accounts for 0.33% of GDP (Fig. A4). In contrast, the EAD of JRB's riverine floods accounts for 0.36% of GDP, higher than the national average. In addition, the results show that when the flood return period is less than 30 years, the overall damage to the basin rises slowly. The total damage increases sharply, however, when the flood return period is over 30 years.

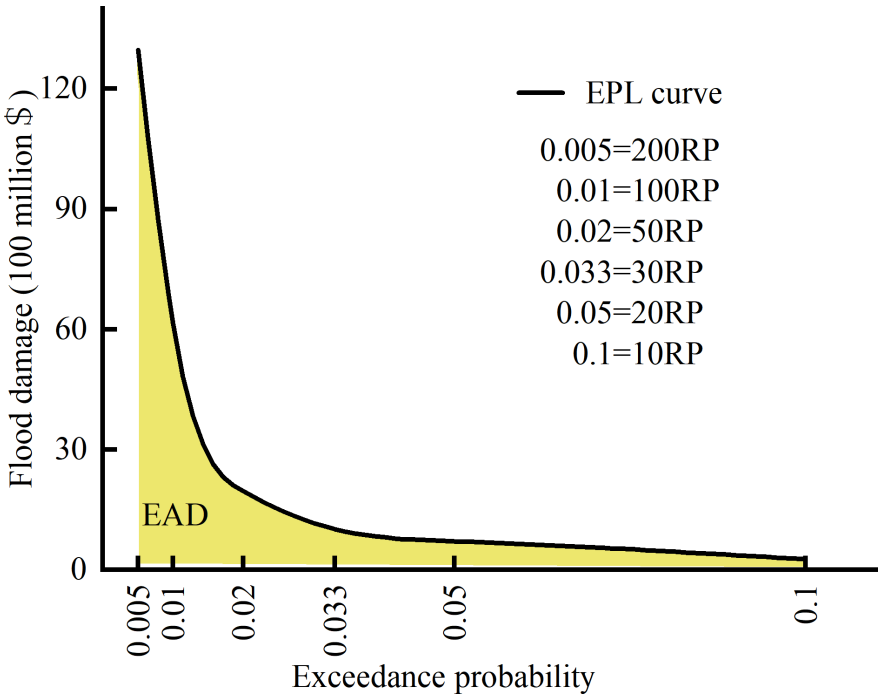

Fig. 6 Damage-probability curve (risk curve) and EAD in the JRB

Fig. 7 shows the spatial distribution of flood risk in the JRB. From this figure, we found that when the flood event had a 10-year return period, the flood risk in the Xinluo district was higher than in the other places in the JRB. The flood risk in Xinluo district was the highest, followed by Longhai city and downtown Zhangzhou. If the flood event occurred during 20-year to 30-year return periods, the flood risk in Longhai city was higher than in any of the other places. The flood risk in Longhai city was the highest, followed by the Xinluo district and downtown Zhangzhou. If the flood event was during 50-year to 200-year return periods, the flood risk in downtown Zhangzhou was higher than in any of the other places. The flood risk in downtown Zhangzhou was the highest, followed by Longhai city and Xinluo city.

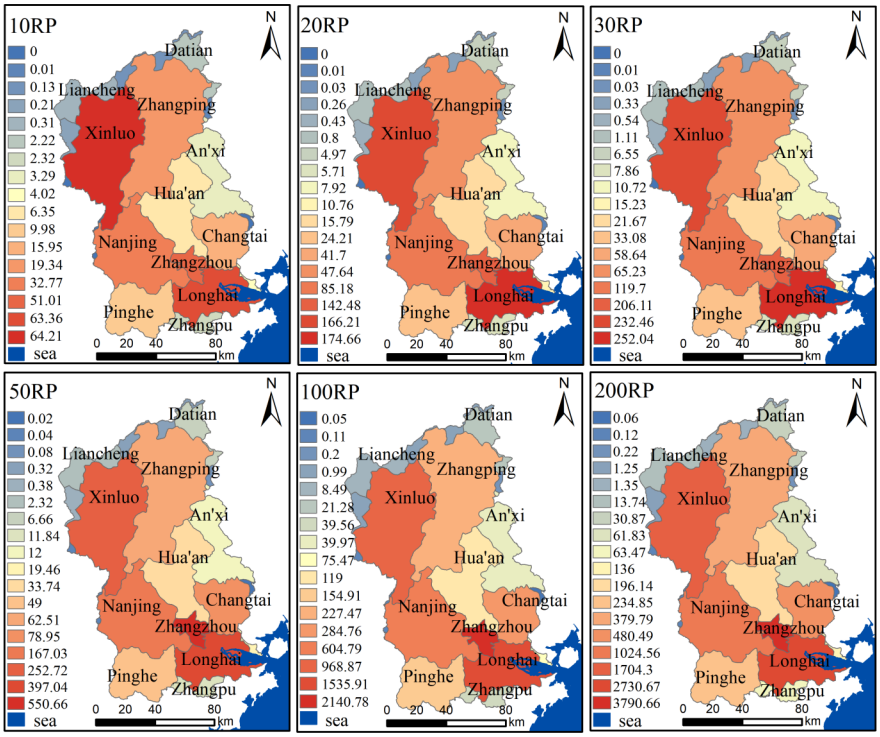

Note: RP represents the return period of a flood event. The values in the figure represent the flood risks for different flood return periods, and the unit of flood risk is millions of dollars.

Fig. 7 Flood risk distribution map in the JRB

Surprisingly, when the flood event is beyond a 20-year return period, the flood risk in the lower reaches of the JRB is higher than in the upper reaches, yet when the flood event is lower than a 20-year return period, the flood risk in the upper reaches of the JRB is higher than in the lower reaches. By comparing the asset exposure, inundated area, and flood damage, as shown in Fig. 8, we found that because the asset exposure in Longyan city in the upstream stretch was larger than in the downstream one, the flood risk upstream was larger than in the downstream in a 10-year return period flood event. However, for a return period above 20 years, the inundated area dominates the change in flood risk. Thus, the flood risk downstream was larger than in the upstream when the return period was over 20 years.

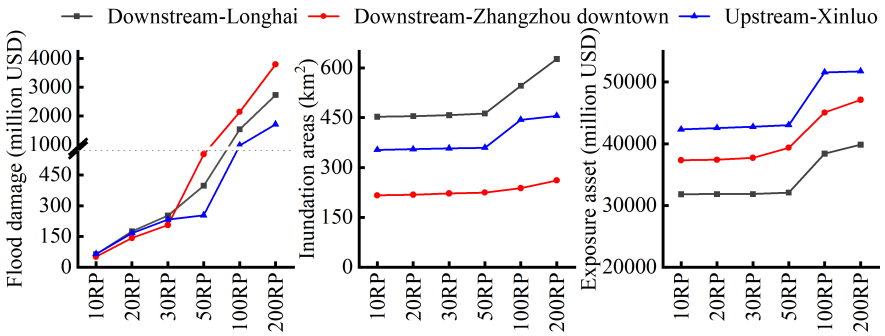

Fig. 8 Asset exposure, inundated areas, and flood damage in the JRB

To reflect the damage in different departments in the JRB, the built-up land area was divided into industrial,

construction, transportation, infrastructure, and tertiary industries, according to the proportion of the population engaged in each industry (Yin et al., 2021). The proportions of the employed population in industrial, tertiary industry, infrastructure, transportation and construction in the JRB are 0.39:0.32:0.01:0.21:0.07. The classification standard is based on the National Economical Industry Classification (GB/T4754-2017). These classifications are in accordance with the categories classified by The damage results caused by floods to different sectors are shown in Fig. 9. In all areas the flood damage increases with the flood return period, but the industrial damage is the largest, followed by the tertiary industry, transportation, construction, agriculture, and infrastructure.

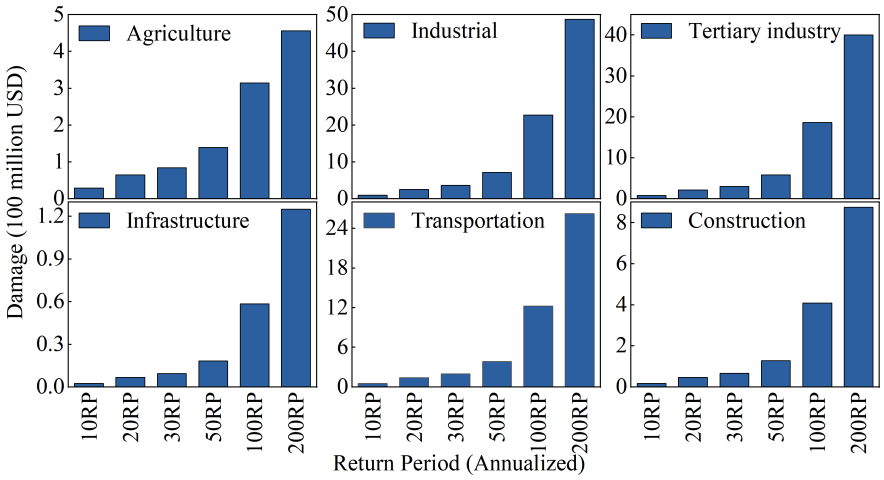

Fig. 9 Estimated damage in the different sectors under various return-period floods

4. Discussion

4.1. Applicability of the combined flood risk models

This study provides a combined flood risk estimation to obtain the EAD and flood risk curve. Most flood-risk models are based on three index systems: hazard, exposure, and vulnerability, limiting their applicability (Lyu et al., 2018; Wang et al., 2021a). The flood risk model combines the HAND model and the damage estimation model. The HAND model simulates the detailed inundation depths according to the digital elevation model, river discharge, and water-level data (Fang et al., 2022). Scenario-based methods can select specific scenarios according to different research needs, such as land cover scenarios at different time scales or different social development scenarios (Yin et al., 2015; Lin et al., 2020). The combined model chain can not only assess flood risk but also simulate the evolution of flood and evaluate the disaster losses (de Moel et al., 2015; Li et al., 2016). The combined flood risk method differs from the statistical equations for fitting historical empirical data. It can use current conditions to analyze the flood risk curves in different return-period floods. In this study, all available information was employed as the input of the scenario design, and this information can be easily replaced by users according to the design of flood inundation maps, in the future. Researchers can update the inundation maps with climate change data, ensuring the applicability and performance of the flood risk model. Therefore, this method can be easily applied to other river basins. Consistent with previous studies, we found that this approach has the same result as using the index system method to assess the flood risk in the JRB, and all of the results indicate a higher flood risk zone located downstream of the JRB (Tang et al., 2020).

4.2. Flood risk response

Through analysis of the land-use and flood inundation maps in the JRB, we found that farmland was the largest flooded area in the floodplain. Due to long-term accumulated experience, humans have adopted some adaptation measures to reduce agricultural flood risk, such as planting water-sensitive crops to adapt to this environment. In addition, humans have raised the ridges nearly 30 cm, to avoid direct inundation of the farmland near rivers or distribution in low-lying fields. However, these adaptations can only cope with regular rainfall. If heavy rainstorm warning news is released in advance, farmers immediately dredge the ridges to allow excess water to flow out. In combination with the diversion canals, reservoirs, and pumps, this measure will decrease the flood risk to farmland.

Through analysis of the damage results of different sectors in the JRB, we found that there are many assets allocated to riverine flood-prone areas. Therefore, improving the flood protection level in flood-prone areas is essential. Previous research has found that agricultural land has decreased and construction land has increased in the JRB (Tang et al., 2020; Tang et al., 2021). Fortunately, it is an interesting result that if built-up land decreases in a flood inundation map, the total damage would decrease in the JRB. Therefore, regulating asset exposure and infrastructure vulnerability in the flooded area, to reduce property damage, is necessary in this watershed. In addition, implementing river management techniques such as regular dredging and inspection of the river can prevent serious silting of the river, which could lead to elevation of the riverbed, reducing flood discharge capacity, water flow, and other natural damage-reducing measures.

4.3. Limitations and validation

There are many uncertainties in the process of flood risk assessment. Pinelli et al. (2020) found that there is inevitable uncertainty in estimating the value of assets. Koks et al. (2019) showed that the economic damage caused by the failure of critical infrastructure might be underestimated. Different regions, receptors, inundation depths, flooding time, and flow velocity will cause different losses (Apel et al., 2004; Merz et al., 2009; de Moel et al., 2011). For example, the depth-damage curves in Britain, Germany, the Netherlands, the United States, Australia, Japan, and Thailand are not all the same. Therefore, the depth-damage curves cited in this article may not directly apply in the JRB, and could increase the uncertainty of the damage results in the study area. Secondly, uncertainty of land-use classification results caused by remote sensing image resolution and uncertainty in asset estimation will also affect the final damage assessment. Finally, the inundation results of riverine floods are also affected by the input parameters of the flood model used (Ahmadisharaf et al., 2019; Jokar et al., 2021). Channel roughness, curvature, flood control measures, and other factors could lead to uncertainty in the HAND model simulation of flood inundation processes.

Super-typhoon Meranti passed through this basin on 15 September 2016, causing a total agricultural damage of 232.36 million USD in the JRB. The typhoon brought heavy rainfall in some areas, with a maximum rainfall of 105 mm in one hour and precipitation of 340 to 467 mm in 24 hours. This extreme rainfall was beyond the 100-year return-period level in some places and a caused a flood more severe than that of an 80-year return period. We found that the agricultural damage from the extreme precipitation events caused by the super-typhoon Meranti differed by 26.12% from the damage caused by our simulated 100-year flood.

4.4. Implications for flood risk management

Life and property have been highly concentrated in the floodplain with the process of urbanization. But riparian buffers contribute to reducing flood risk (McLean et al., 2015). Gregory et al. (1990) found that a riparian buffer zone should cover the whole 100-year return period floodplain; otherwise, serious flood damage will occur. This study shows that the total damage increased sharply over the 30-year return period of flood events; obviously, establishing a floodplain is not enough in the JRB. In addition, the inundated area and asset exposure in the JRB have increased as the flood return period has increased. Therefore, it is necessary to adjust the land-use structure to optimal proportions or reduce the intensity of human activities and asset exposure on both sides of the river, to minimize major economic damage.

The combined effects of climate change and underlying surface conditions of land-use change have made the problem of flood disasters increasingly complicated, and flood management is becoming more and more important. Flood risk management should focus on avoiding new risks, increasing watershed resilience and flood awareness, and reducing flood damage and impacts (Fekete et al., 2020). Due to the uncertainty and unmanageability of flood risk, the government should strengthen comprehensive disaster management and build a disaster management framework from five aspects: prevention, defense, mitigation, response, and recovery, to reduce, avoid, regulate, and resist flood risk (Morrison et al., 2019; Guerriero et al., 2021). At the same time, a comprehensive flood forecast, early warning, dispatch, emergency disaster relief, evacuation plan, and post-disaster reconstruction system should be established to manage the entire process of flood disasters.

Generally, engineering measures keep floods away from humans, and non-engineering measures keep humans away from floods (Peacock and Husein, 2011). Nature-based solutions are an effective approach, ensuring that the benefits will increase over time. Riparian buffer zones are one of the nature-based solutions. Unlike engineering measures such as dams and reservoirs, buffers have no service life limit. Although the initial investment cost of a riparian buffer zone is relatively high, its subsequent maintenance cost is relatively low, so that its marginal benefit will gradually increase over time. Nevertheless, this does not mean gray engineering measures are not also effective; Ward et al. (2017), for example, showed that to reduce flood risk, dykes were a more attractive solution. Any one type of flood-control measure is not enough in itself to solve the flood disaster problem. Once a flood exceeding the standard occurs, it will cause problems such as dam failure, dyke burst, infrastructure failure, etc., which will increase the impact of flood disasters on human life and property. In order to reduce the impact of flood disasters on human life and property most effectively, we should adopt different flood management measures, according to the characteristics of the flood-prone areas. It is best to choose a hybrid solution to reduce riverine flooding while avoiding the option of irreversible flood management measures.

5. Conclusions

A flood risk curve can provide a better outcome while also performing EAD more quickly. This study developed a combined riverine flood risk model for quantifying the risk change in the JRB. Findings from flood damage analysis revealed that the EAD of riverine floods accounts for 0.36% of GDP in JRB, higher than the average level in China. From the risk curve in the JRB, we can find when the flood return period is larger than 30 years, the total damage increases sharply. The main findings imply that the riverine flood protection level appears to be a nearly 30-year return period in the JRB. Hence, flood adaptation should focus on improving the 30-year return period protection level. The risk map illustrates that the overall risk level is inconsistent; therefore, it is necessary to narrow the flood protection gaps between the upstream and downstream areas, and relieve the flood control pressure downstream.

Moreover, climate change and the ongoing urbanization process will exacerbate the human impact of flood disasters, if flood risk is improperly managed. By analyzing asset exposure, land use cover, and inundation maps, we suggest adjusting the land-use structure, implementing a hybrid management strategy, and avoiding choosing irreversible management measures while at the same time reducing the probability of flooding on the underlying surface, and the exposure and vulnerability of receptors. Finally, the empirical findings of this study can provide decision makers with more informative support in disaster prevention, expected loss, and flood management planning.

Acknowledgments We thank the funding support by the National Natural Science Foundation of China (Grant Nos.: 41661144032), the international partnership program of the Chinese Academy of Sciences “Multifunctional urban green space planning based on transdisciplinary learning” (Grant Nos.: 132C35KYSB20200007).

Appendix

Appendix figures

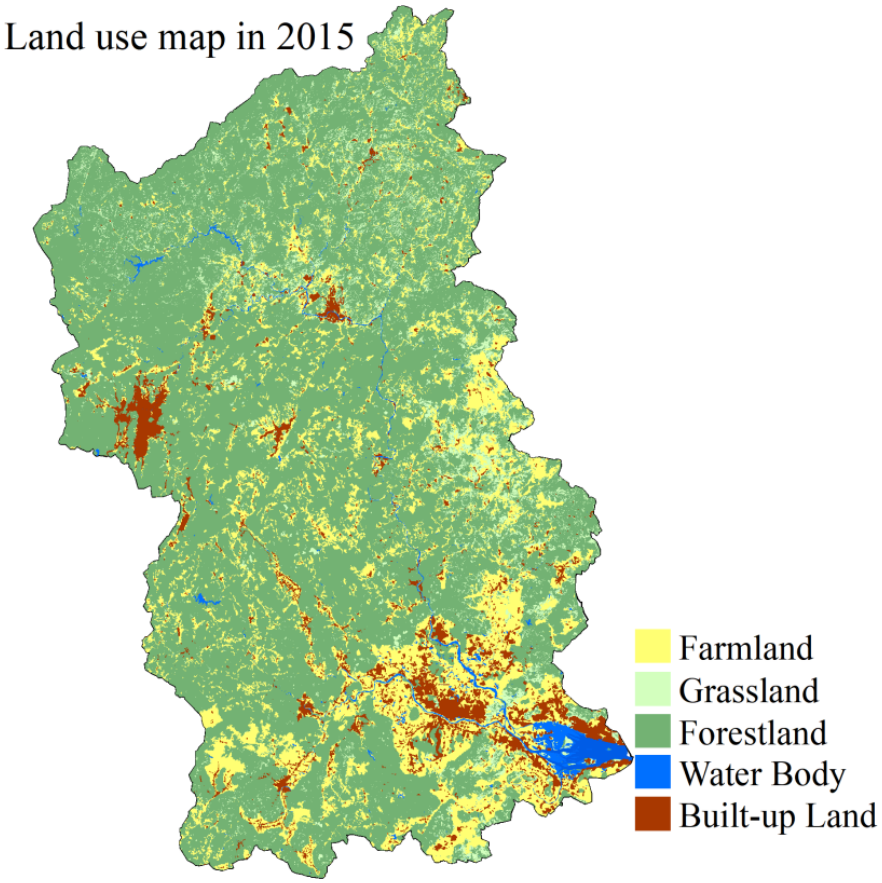

Fig. A1 Land use map in the JRB

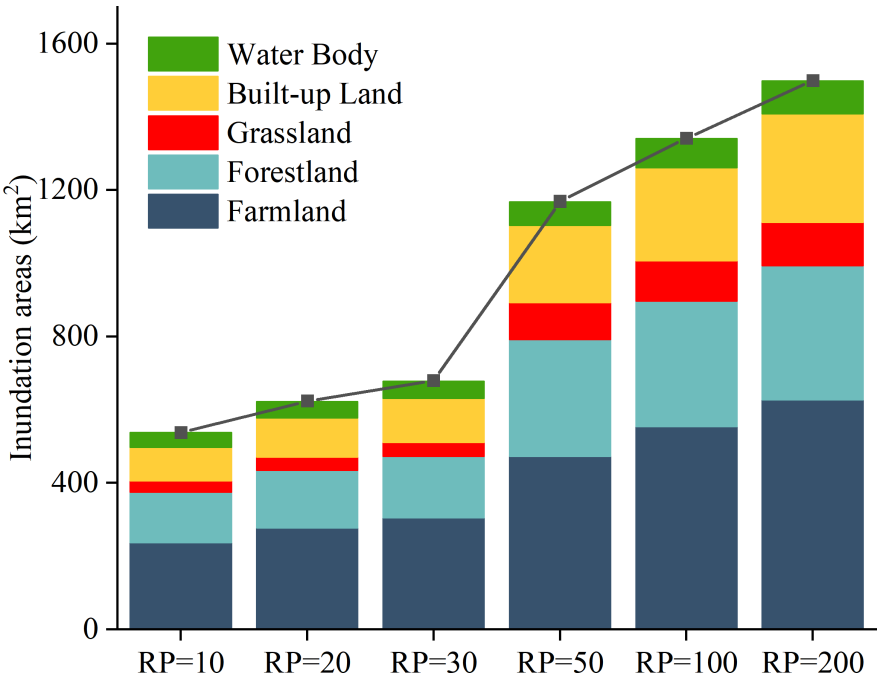

Fig. A2 Flood inundation map of different land-use types

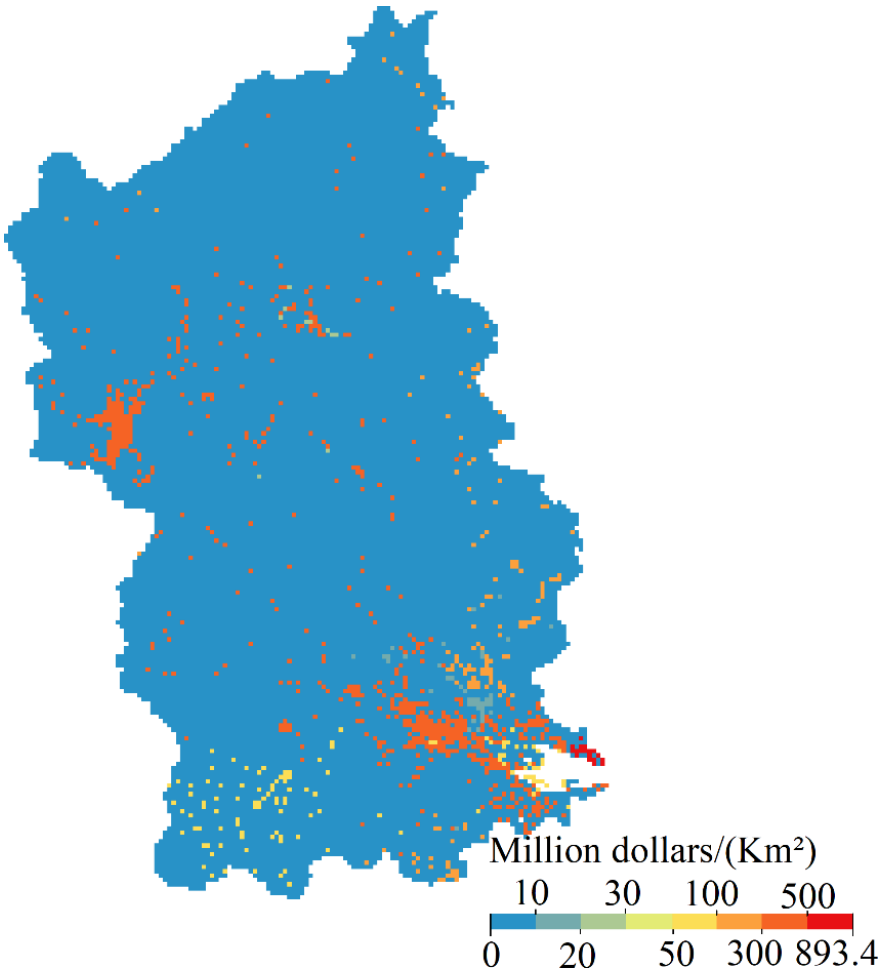

Fig. A3 Unit values of land in the JRB

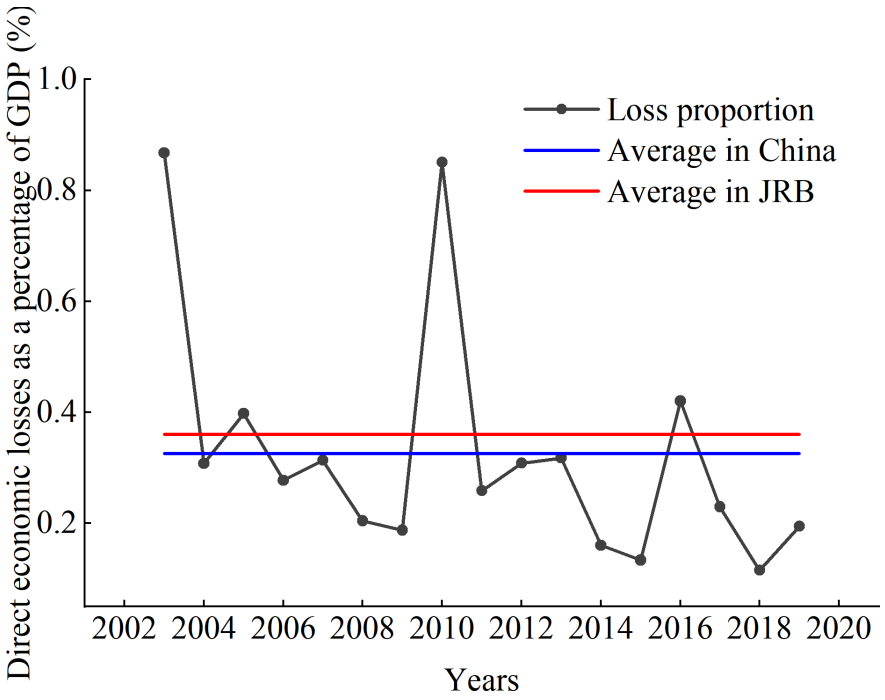

Fig. A4 Direct economic losses caused by floods as a percentage of GDP

Appendix tables

Table A1 Inundation land areas in different flood return periods

Land use (km^2)	Return periods	Return periods	Return periods	Return periods	Return periods	Return periods
	10	20	30	50	100	200
Farmland	237.10	277.29	304.88	472.87	554.08	627.96
Forestland	138.02	157.04	167.61	318.47	342.96	365.80
Grassland	31.60	36.03	38.21	100.98	109.59	117.98
Built-up Land	90.13	107.43	120.49	211.27	254.07	295.53
Water Body	41.20	45.39	48.16	65.05	79.84	90.90

Table A2 Unit value of farmland and built-up land (million dollars/km^2)

	Farmland	Built-up Land
Xinluo District	2.84	363.81
Zhangping City	4.80	335.02
Shanghang County	3.85	325.99
Liancheng County	6.11	141.16
Yongding County	3.62	266.91
Zhangzhou City	6.10	392.95
Longhai City	6.23	309.49
Changtai County	5.12	229.18
Nanjing County	9.05	355.20
Hua'an County	9.62	315.15

	Farmland	Built-up Land
Pinghe County	9.90	85.54
Zhangpu County	6.25	142.66
Haicang District	1.12	893.34
Tong'an District	2.71	221.41
Anxi County	6.28	233.00
Yongchun County	6.32	559.28
Datian County	7.31	271.57
Yong'an City	4.21	358.60

References

Aerts, J. C., Botzen, W. J., Clarke, K. C., Cutter, S. L., Hall, J. W., Merz, B., Kunreuther, H. 2018. Integrating human behaviour dynamics into flood disaster risk assessment. Nature Climate Change, 8(3), 193-199. https://doi.org/10.1038/s41558-018-0085-1.

Ahmadisharaf, E., Kalyanapu, A. J. 2019. A coupled probabilistic hydrologic and hydraulic modelling framework to investigate the uncertainty of flood loss estimates. Journal of Flood Risk Management, 12(S2): e12536. https://doi.org/10.1111/jfr3.12536.

Apel, H., Thieken, A. H., Merz, B., Bloschl, G. 2004. Flood risk assessment and associated uncertainty. Natural Hazards and Earth System Sciences, 4(2): 295-308. https://doi.org/10.5194/nhess-4-295-2004.

Bellos, V., Tsakiris, G. 2016. A hybrid method for flood simulation in small catchments combining hydrodynamic and hydrological techniques. Journal of Hydrology, 540, 331-339. https://doi.org/10.1016/j.jhydrol.2016.06.040

Bloschl, G., Hall, J., Parajka, J., Perdigao, R. A. P., Merz, B., Arheimer, B., Aronica, G. T., Bilibashi, A., Bonacci, O., Borga, M., Canjevac, I., Castellarin, A., Chirico, G. B., Claps, P., Fiala, K., Frolova, N., Gorbachova, L., Gul, A., Hannaford, J., Harrigan, S., Kireeva, M., Kiss, A., Kjeldsen, T. R., Kohnova, S., Koskela, J. J., Ledvinka, O., Macdonald, N., Mavrova-Guirguinova, M., Mediero, L., Merz, R., Molnar, P., Montanari, A., Murphy, C., Osuch, M., Ovcharuk, V., Radevski, I., Rogger, M., Salinas, J. L., Sauquet, E., Sraj, M., Szolgay, J., Viglione, A., Volpi, E., Wilson, D., Zaimi, K., Zivkovic, N. 2017. Changing climate shifts timing of European floods. Science, 357(6351), 588-590. https://doi.org/10.1126/science.aan2506.

Buchecker, M., Salvini, G., Di Baldassarre, G., Semenzin, E., Maidl, E., Marcomini, A. (2013). The role of risk perception in making flood risk management more effective. Natural Hazards and Earth System Sciences, 13(11), 3013-3030. https://doi.org/10.5194/nhess-13-3013-2013.

CRED (The Centre for Research on the Epidemiology of Disasters) and UNISDR (The UN Office for Disaster Risk Reduction). 2020. Human cost of disasters. An overview of the last 20 years 2000-2019.UN.

de Moel, H., Aerts, J. C. J. H. 2011. Effect of uncertainty in land use, damage models and inundation depth on flood damage estimates. Natural Hazards, 58(1): 407-425. https://doi.org/10.5194/nhess-13-3013-2013.

de Moel, H., Jongman, B., Kreibich, H., Merz, B., Penning-Rowsell, E., Ward, P. J. 2015. Flood risk assessments at different spatial scales. Mitigation and Adaptation Strategies for Global Change, 20(6), 865-890. https://doi.org/10.1007/s11027-015-9654-z.

de Paiva, R. C. D., Buarque, D. C., Collischonn, W., Bonnet, M.-P., Frappart, F., Calmant, S., Bulhões Mendes, C. A. 2013. Large-scale hydrologic and hydrodynamic modeling of the Amazon River basin. Water Resources Research, 49(3), 1226-1243. https://doi.org/10.1002/wrcr.20067

Dottori, F., Szewczyk, W., Ciscar, J. C., Zhao, F., Alfieri, L., Hirabayashi, Y., Bianchi, A., Mongelli, I., Frieler, K., Betts, R. A., Feyen, L. 2018. Increased human and economic losses from river flooding with anthropogenic warming. Nature Climate Change, 8(9): 781-786. https://doi.org/10.1038/s41558-018-0257-z.

Fang, L., Huang, J., Cai, J., Nitivattananon, V. 2022. Hybrid approach for flood susceptibility assessment in a flood-prone mountainous catchment in China. Journal of Hydrology, 612: 1-18.

Fang, L. 2021. Multi-scale flood simulation and management based on rapid flood models and machine learning methods. Xiamen University (in Chinese). https://doi.org/10.1016/j.jhydrol.2022.128091.

Fekete, A., Hartmann, T., Jupner, R. 2020. Resilience: On-going wave or subsiding trend in flood risk research and practice? Wiley Interdisciplinary Reviews-Water, 7(1), e1397. https://doi.org/10.1002/wat2.1397.

Fernandez, D. S., Lutz, M. A. 2010. Urban flood hazard zoning in Tucuman Province, Argentina, using GIS and multicriteria decision analysis. Engineering Geology, 111(1-4), 90-98. https://doi.org/10.1016/j.enggeo.2009.12.006.

Garousi-Nejad, I., Tarboton, D. G., Aboutalebi, M., Torres-Rua, A. F. 2019. Terrain analysis enhancements to the height above nearest drainage flood inundation mapping method. Water Resources Research, 55(10): 7983-8009. https://doi.org/10.1029/2019wr024837.

Gregory, S., Ashkenas, L. 1990. Riparian management guide. Willamette Natioual Forest. US Government Printing Office, Washington, DC, 1990-591-401/35008, 120 pp. (Accessed 20 Jan 2021).

Guerriero, R., Penning-Rowsell, E. C. 2021. Innovation in flood risk management: An 'Avenues of Innovation' analysis. Journal of Flood Risk Management, 14(1), 1-14. https://doi.org/10.1111/jfr3.12677.

Hosseinzadehtalaei, P., Ishadi, N. K., Tabari, H., Willems, P. 2021. Climate change impact assessment on pluvial flooding using a distribution-based bias correction of regional climate model simulations. Journal of Hydrology, 598: 126239. https://doi.org/10.1016/j.jhydrol.2021.126239.

Huizinga, J., Moel, H. de, Szewczyk, W. 2017. Global flood depth-damage functions. Methodology and the database with guidelines. EUR 28552 EN. (Accessed 15 Jan 2021).

ICPR (Intergovernmental Panel on Climate Change), 2001. Atlas of flood danger and potential damage due to extreme floods of the Rhine, International Commission for the Protection of the Rhine, Koblenz.

IPCC (Intergovernmental Panel on Climate Change), 2021. Climate change 2021, the physical science basis. Cambridge: Cambridge University Press.

Jokar, E., Arman, A., & Azari, A. 2021. Forecast and risk analysis of floodplain regarding uncertainty factors. Natural Hazards, 107(2), 1125-1148. https://doi.org/10.1007/s11069-021-04621-z.

Jongman, B., Ward, P. J., Aerts, J. 2012. Global exposure to river and coastal flooding: Long term trends and changes. Global Environmental Change-Human and Policy Dimensions, 22(4): 823-835. https://doi.org/10.1016/j.gloenvcha.2012.07.004.

Koks, E., Pant, R., Thacker, S. Hall, J. W., 2019. Understanding business disruption and economic losses due to electricity failures and flooding. International Journal of Disaster Risk Science, 10(4): 421-438. https://doi.org/10.1007/s13753-019-00236-y.

Li, H. C., Kuo, S. Y., Chen, W. B., Lin, L. Y. 2019. Benefit analysis of flood adaptation under climate change scenario. Natural Hazards, 95(3): 547-568. https://doi.org/10.1007/s11069-018-3500-z.

Li, W. J., Xu, B., Wen, J. H. 2016. Scenario-based community flood risk assessment: a case study of Taining county town, Fujian province, China. Natural Hazards, 82(1), 193-208. https://doi.org/10.1007/s11069-016-2187-2.

Lin, W. B., Sun, Y. M., Nijhuis, S., Wang, Z. L. 2020. Scenario-based flood risk assessment for urbanizing deltas using future land-use simulation (FLUS): Guangzhou Metropolitan Area as a case study. Science of the Total Environment, 739, 139899. https://doi.org/10.1016/j.scitotenv.2020.139899.

Lyu, H. M., Sun, W. J., Shen, S. L., Arulrajah, A. 2018. Flood risk assessment in metro systems of mega-cities using a GIS-based modeling approach. Science of the Total Environment, 626, 1012-1025. https://doi.org/10.1016/j.scitotenv.2018.01.138.

McLean, L., Beevers, L., Wilkinson, M., Starrs, G., Pender, G. 2015. Riparian buffer hydrology: Representing catchment-wide implementation and the influence on flood risk. 36th IAHR World Congress, Delft, Netherlands.

Merz, B., Kreibich, H., Schwarze, R., Thieken, A. 2010. Review article 'Assessment of economic flood damage'. Natural Hazards and Earth System Sciences, 10(8), 1697-1724. https://doi.org/10.5194/nhess-10-1697-2010.

Merz, B., Thieken, A. H. 2009. Flood risk curves and uncertainty bounds. Natural Hazards, 51(3), 437-458. https://doi.org/10.1007/s11069-009-9452-6.

Molinari, D., Dazzi, S., Gattai, E., Minucci, G., Pesaro, G., Radice, A., Vacondio, R. 2021. Cost-benefit analysis of flood mitigation measures: a case study employing high-performance hydraulic and damage modelling. Natural Hazards, 108(3): 3061-3084. https://doi.org/10.1007/s11069-021-04814-6.

Morrison, A., Noble, B. F., Westbrook, C. J. 2019. Flood Risk Management in Canada's Prairie Provinces: an Analysis of Decision-Maker Priorities and Policy Preferences. Environmental Management, 64(5), 608-625. https://doi.org/10.1007/s00267-019-01208-0.

Nobre, A. D., Cuartas, L. A., Momo, M. R., Severo, D. L., Pinheiro, A., Nobre, C. A. 2016. HAND contour: a new proxy predictor of inundation extent. Hydrological Processes 30(2): 320-333. https://doi.org/10.1002/hyp.10581.

Peacock, W. G., Husein, R., Center, R. 2011. The adoption and implementation of hazard mitigation policies and strategies by coastal jurisdictions in Texas: The planning survey results. Texas A&M University Hazard Reduction and Recovery Center. (Accessed 13 Dec 2020)

Pinelli, J.-P., Da Cruz, J., Gurley, K., Paleo-Torres, A. S., Baradaranshoraka, M., Cocke, S., Shin, D. 2020. Uncertainty reduction through data management in the development, validation, calibration, and operation of a hurricane vulnerability model. International Journal of Disaster Risk Science, 11(6): 790-806. https://doi.org/10.1007/s13753-020-00316-4.

Roy, B., Khan, M. S. M., Islam, A., Khan, M. J. U., Mohammed, K. 2021. Integrated flood risk assessment of the Arial Khan River under changing climate using IPCC AR5 risk framework. Journal of Water and Climate Change, 12(7), 3421-3447. https://doi.org/10.2166/wcc.2021.341.

Shrestha, M. S., Gurung, M. B., Khadgi, V. R., Wagle, N., Banarjee, S., Sherchan, U., Parajuli, B., Mishra, A. 2021. The last mile: Flood risk communication for better preparedness in Nepal. International Journal of Disaster Risk Reduction, 56: 102118. https://doi.org/10.1016/j.ijdrr.2021.102118.

Tang, J. X., Li, Y. M., Cui, S. H., Xu, L. L., Ding, S. P., Nie, W. 2020. Linking land-use change, landscape patterns, and ecosystem services in a coastal watershed of southeastern China. Global Ecology and Conservation, 23: e01177. https://doi.org/10.1016/j.gecco.2020.e01177.

Tang, J. X., Li, Y. M., Cui, S. H., Xu, L. L., Hu, Y. C., Ding, S. P., Nitivattananon, V. 2021. Analyzing the spatiotemporal dynamics of flood risk and its driving factors in a coastal watershed of southeastern China. Ecological Indicators, 121: 107134. https://doi.org/10.1016/j.ecolind.2020.107134.

Tehrany, M. S., Pradhan, B., Jebur, M. N. 2014. Flood susceptibility mapping using a novel ensemble weights-of-evidence and support vector machine models in GIS. Journal of Hydrology, 512, 332-343. https://doi.org/10.1016/j.jhydrol.2014.03.008.

Wang, G. P., Liu, L. Y., Shi, P. J., Zhang, G. M., Liu, J. F. 2021a. Flood Risk Assessment of Metro System Using Improved Trapezoidal Fuzzy AHP: A Case Study of Guangzhou. Remote Sensing, 13(24), 5154. https://doi.org/10.3390/rs13245154.

Wang, H., Zhou, J., Tang, Y., Liu, Z., Kang, A., Chen, B. 2021b. Flood economic assessment of structural measure based on integrated flood risk management: A case study in Beijing. Journal of Environmental Management, 280, 111701. https://doi.org/10.1016/j.jenvman.2020.111701.

Ward, P. J., Jongman, B., Aerts, J., Bates, P. D., Botzen, W. J. W., Loaiza, A. D., Hallegatte, S., Kind, J. M., Kwadijk, J., Scussolini, P., Winsemius, H. C. 2017. A global framework for future costs and benefits of river-flood protection in urban areas. Nature Climate Change, 7(9): 642-648. https://doi.org/10.1038/nclimate3350.

Win, S., Zin, W. W., Kawasaki, A., San, Z. M. L. T. 2018. Establishment of flood damage function models: A case study in the Bago River Basin, Myanmar. International Journal of Disaster Risk Reduction, 28, 688-700. https://doi.org/10.1016/j.ijdrr.2018.01.030.

Wu, J., Li, N., Shi, P. 2014. Benchmark wealth capital stock estimations across China's 344 prefectures: 1978 to 2012. China Economic Review, 31: 288-302. https://doi.org/10.1016/j.chieco.2014.10.008.

Wu, J. D., Wang, C. L., He, X., Wang, X., Li, N. 2017. Spatiotemporal changes in both asset value and GDP associated with seismic exposure in China in the context of rapid economic growth from 1990 to 2010. Environmental Research Letters, 12(3): 034002. https://doi.org/10.1088/1748-9326/aa5d47.

Wu, X. H., Zhou, L., Gao, G., Guo, J., Ji, Z. H. 2016. Urban flood depth-economic loss curves and their amendment based on resilience: evidence from Lizhong Town in Lixia River and Houbai Town in Jurong River of China. Natural Hazards, 82(3): 1981-2000. https://doi.org/10.1007/s11069-016-2281-5.

Wu, Z. N., Lv, H., Meng, Y., Guan, X. J., Zang, Y. W. 2021. The determination of flood damage curve in areas lacking disaster data based on the optimization principle of variation coefficient and beta distribution. Science of the Total Environment, 750, 13, 142277. https://doi.org/10.1016/j.scitotenv.2020.142277.

Yang, Y., Sun, L., Li, R., Yin, J., Yu, D. 2020. Linking a storm water management model to a novel two-dimensional model for urban pluvial flood modeling. International Journal of Disaster Risk Science, 11(4): 508-518. https://doi.org/10.1007/s13753-020-00278-7.

Ye, M. Q., Wu, J. D., Wang, C. L., He, X. 2019. Historical and future changes in asset value and GDP in areas exposed to tropical cyclones in China. Weather Climate and Society, 11(2): 307-319. https://doi.org/10.1175/wcas-d-18-0053.1.

Yildirim, E., Demir, I. 2021. An Integrated Flood Risk Assessment and Mitigation Framework: A Case Study for Middle Cedar River Basin, Iowa, US. International Journal of Disaster Risk Reduction, 56, 102113. https://doi.org/10.1016/j.ijdrr.2021.102113.

Yin, J., Yu, D. P., Yin, Z. N., Wang, J., Xu, S. Y. 2015. Modelling the anthropogenic impacts on fluvial flood risks in a coastal mega-city: A scenario-based case study in Shanghai, China. Landscape and Urban Planning, 136, 144-155. https:/doi.org/10.1016/j.landurbplan.2014.12.009.

Yin, Z., Hu, Y., Jenkins, K., He, Y., Forstenhäusler, N., Warren, R., Yang, L., Jenkins, R., Guan, D. 2021. Assessing the economic impacts of future fluvial flooding in six countries under climate change and socio-economic development. Climatic Change, 166(3-4). https://doi.org/10.1007/s10584-021-03059-3.

Yin, Z. E., Yin, J., Xu, S. Y., Wen, J. H. 2011. Community-based scenario modelling and disaster risk assessment of urban rainstorm waterlogging. Journal of Geographical Sciences, 21(2), 274-284. https://doi.org/10.1007/s11442-011-0844-7.

Zhang, H. P., Wu, W. M., Hu, C. H., Hu, C. W., Li, M., Hao, X. L., Liu, S. 2021a. A distributed hydrodynamic model for urban storm flood risk assessment. Journal of Hydrology, 600, 126513. https://doi.org/10.1016/j.jhydrol.2021.126513.

Zhang, W., Villarini, G., Vecchi, G. A., Smith, J. A. 2018. Urbanization exacerbated the rainfall and flooding

caused by hurricane Harvey in Houston. Nature, 563(7731): 384-388. https://doi.org/10.1038/s41586-018-0676-z.

Zhang, W. X., Furtado, K., Wu, P. L., Zhou, T. J., Chadwick, R., Marzin, C., Rostron, J., Sexton, D. 2021b. Increasing precipitation variability on daily-to-multiyear time scales in a warmer world. Science Advances, 7(31): eabf8021. https:/doi.org/10.1126/sciadv.abf8021.

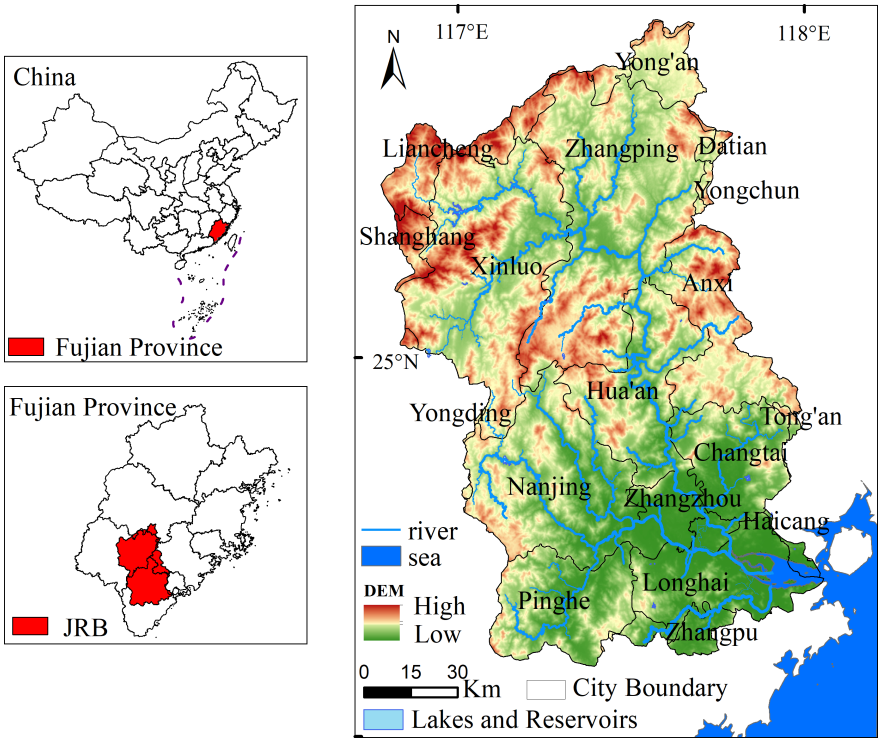

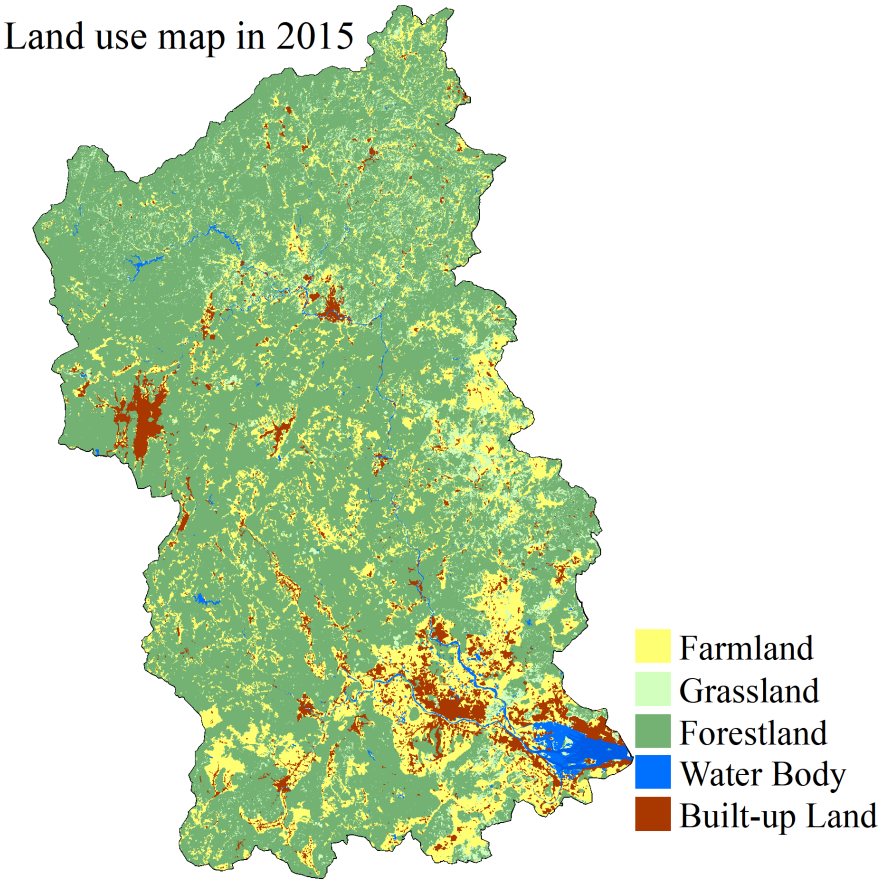

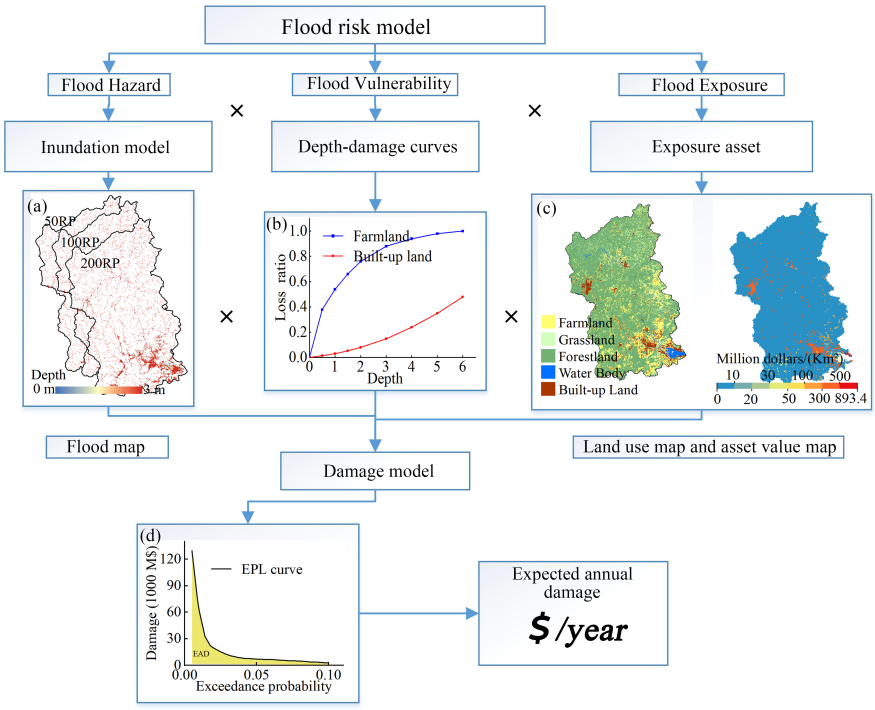

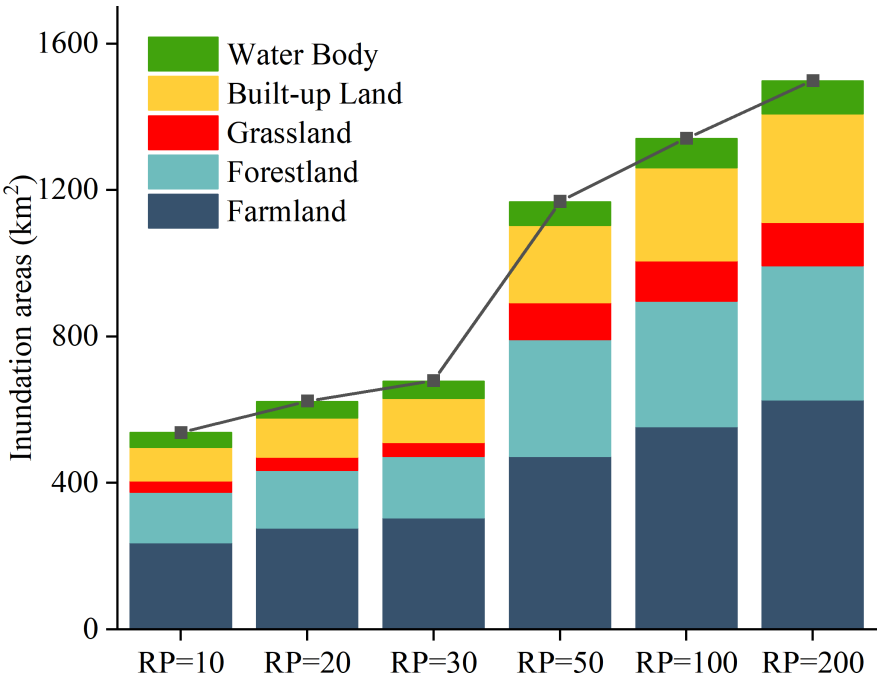

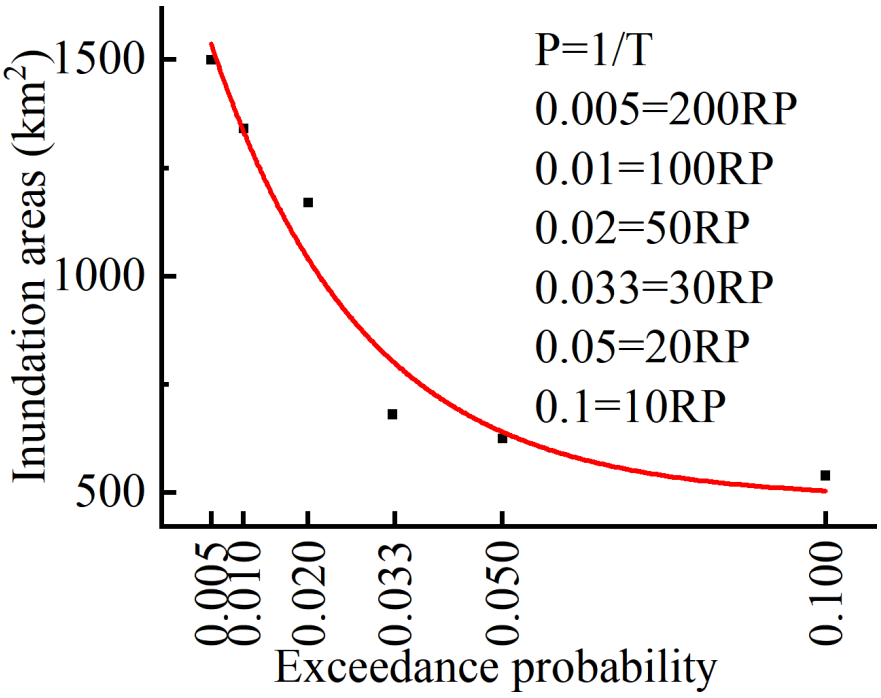

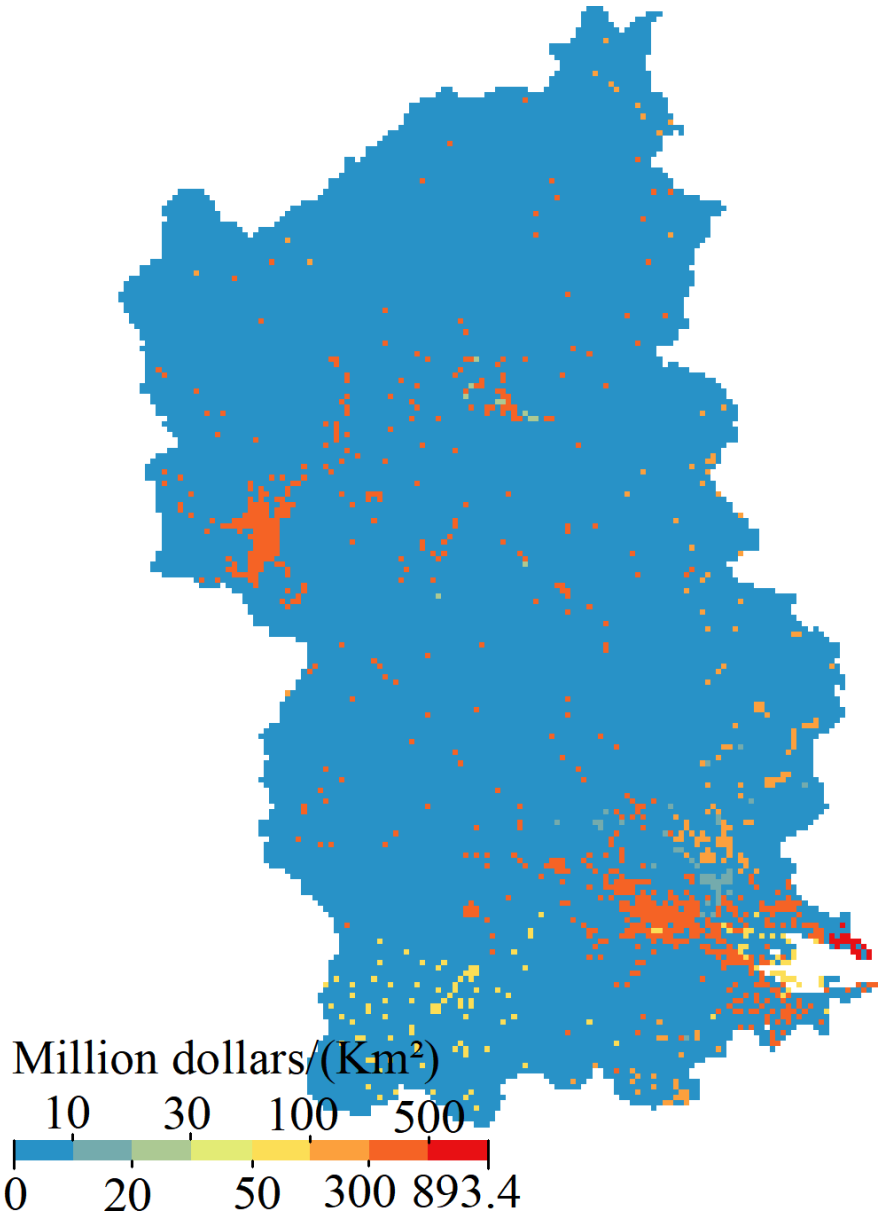

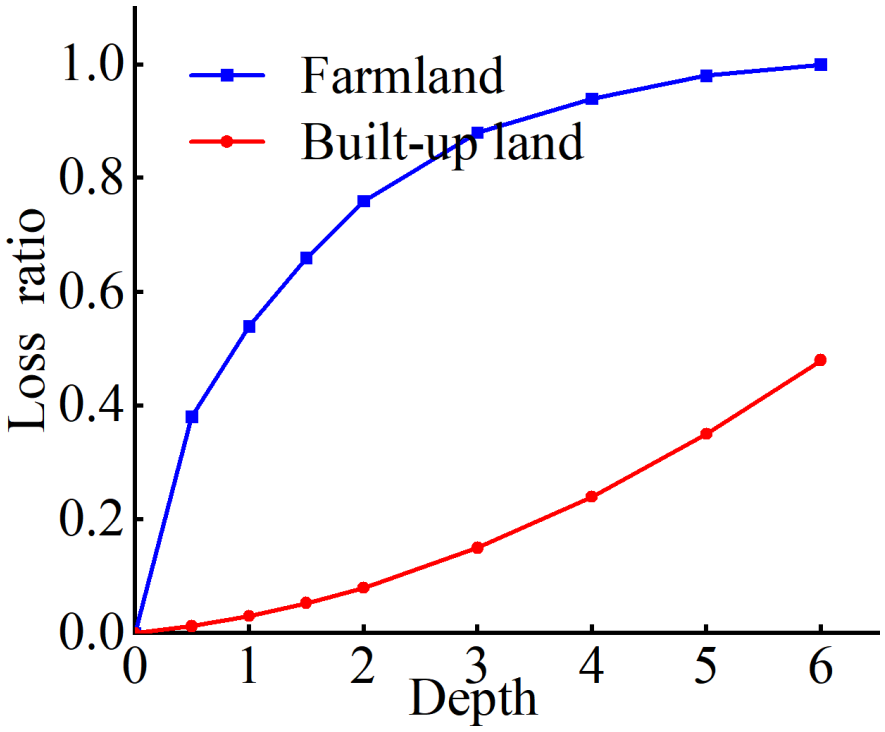

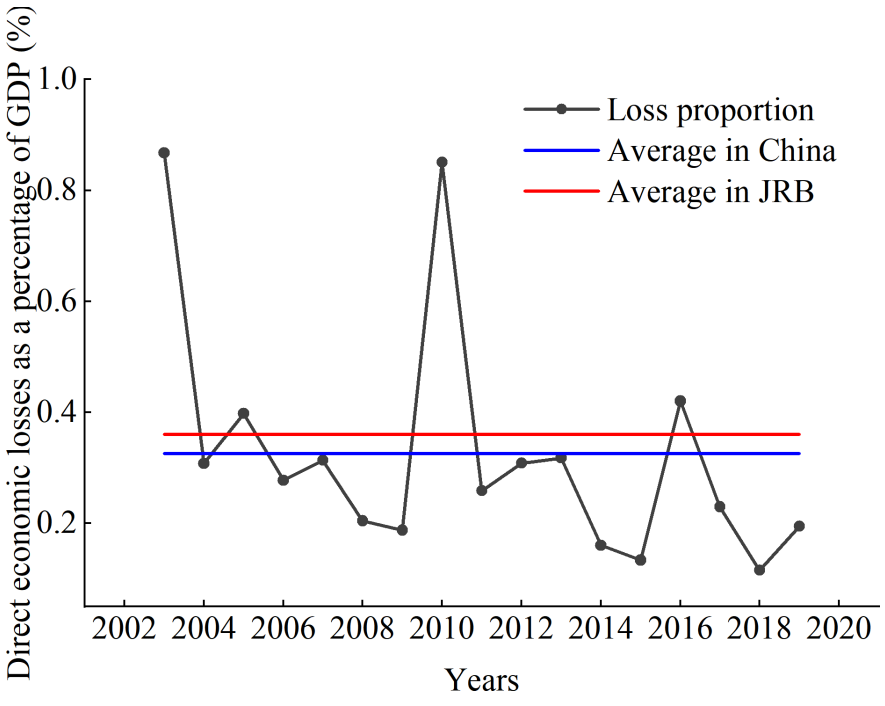

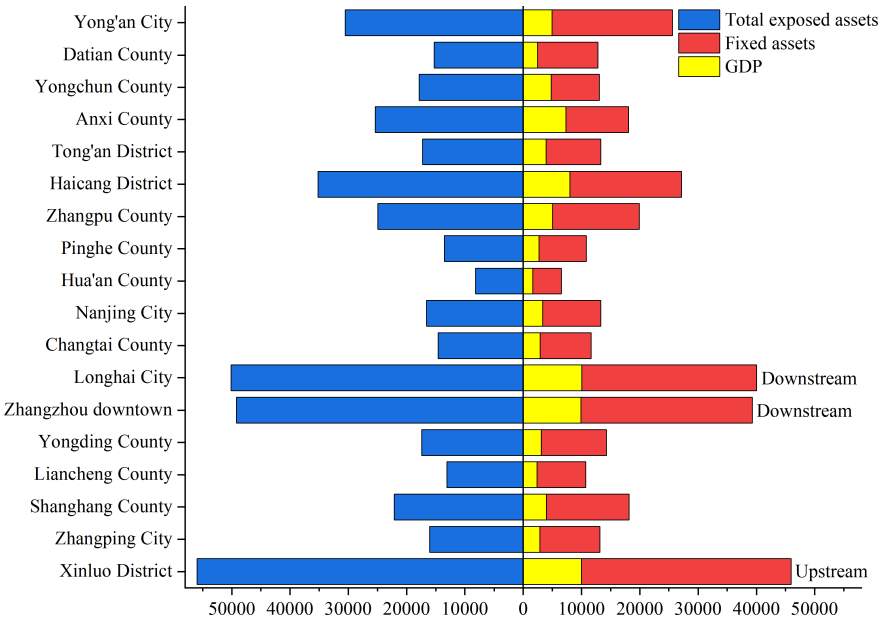

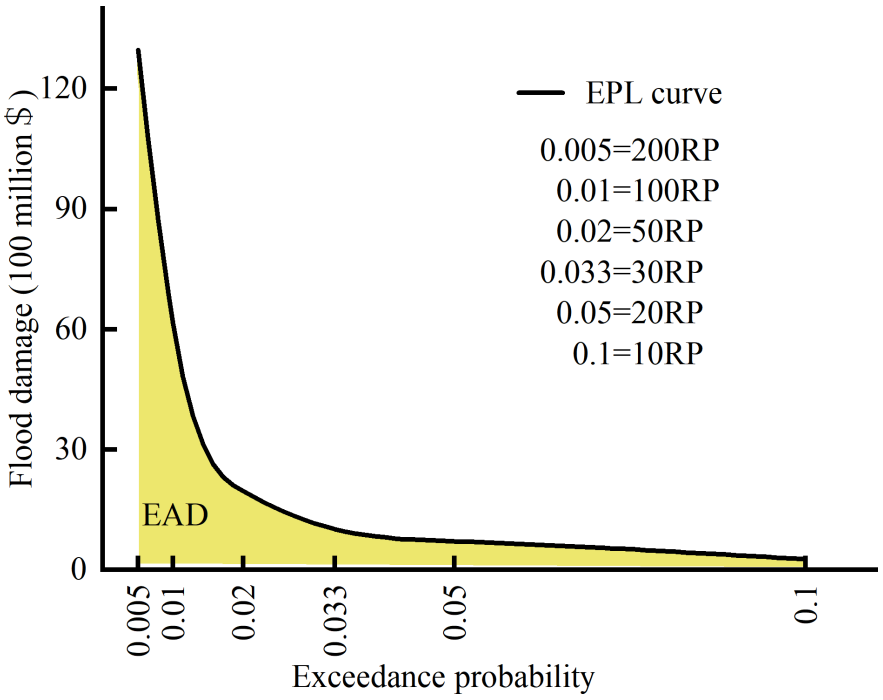

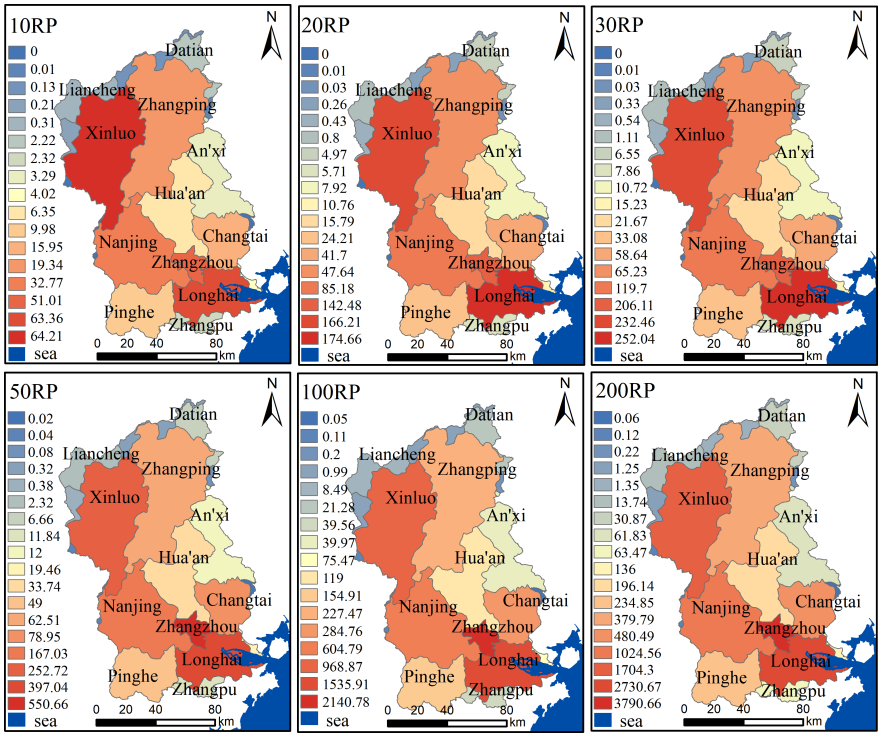

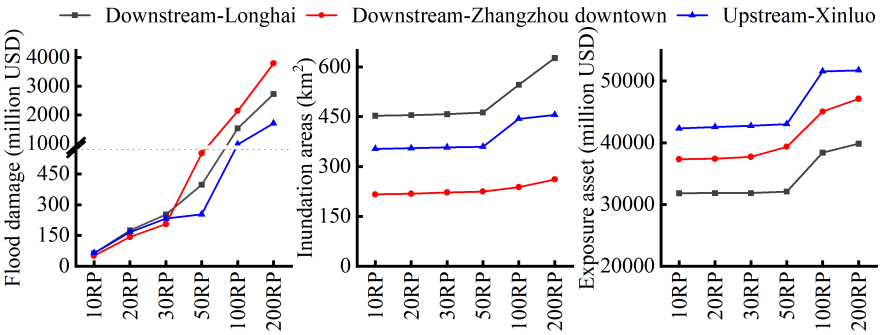

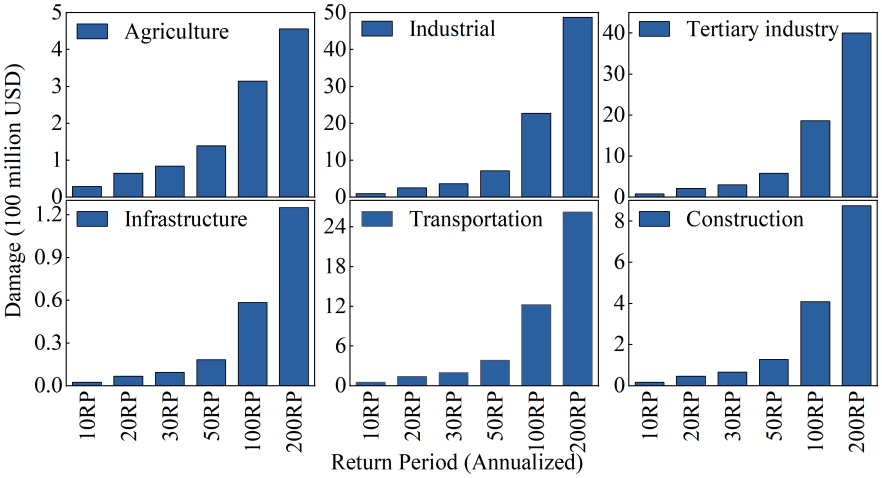

Hosted file

`Table.docx` available at https://authorea.com/users/584733/articles/623802-riverine-flood-risk-assessment-with-a-combined-model-chain-in-southeastern-china